Optics Letters

Efficient non-line-of-sight tracking with computational neuromorphic imaging

SHUO ZHU,[1,2] ZHOU GE,[1,3] CHUTIAN WANG,[1] JING HAN,[2,4] AND EDMUND Y. LAM[1,*]

[1]Department of Electrical and Electronic Engineering, The University of Hong Kong, Pokfulam, Hong Kong SAR, China
[2]School of Electronic and Optical Engineering, Nanjing University of Science and Technology, Nanjing, Jiangsu Province 210094, China
[3]School of Mechatronic Engineering and Automation, Shanghai University, Shanghai 200444, China
[4]eohj@njust.edu.cn
*elam@eee.hku.hk

Received 14 May 2024; revised 7 June 2024; accepted 9 June 2024; posted 10 June 2024; published 18 June 2024

Non-line-of-sight (NLOS) sensing is an emerging technique that is capable of detecting objects hidden behind a wall, around corners, or behind other obstacles. However, NLOS tracking of moving objects is challenging due to signal redundancy and background interference. Here, we demonstrate computational neuromorphic imaging with an event camera for NLOS tracking, unaffected by the relay surface, which can efficiently obtain non-redundant information. We show how this sensor, which responds to changes in luminance within dynamic speckle fields, allows us to capture the most relevant events for direct motion estimation. The experimental results confirm that our method has superior performance in terms of efficiency, and accuracy, which greatly benefits from focusing on well-defined NLOS object tracking.

https://doi.org/10.1364/OL.530066

The capability of traditional optical imaging has been vastly extended via computational approaches, which combine detection and processing methods to form images even when the sensing conditions are complex and highly indirect [1,2]. Recent years have witnessed tremendous advances in non-line-of-sight (NLOS) imaging techniques, which have broad sensing applications encompassing image reconstruction, object tracking, depth imaging, posture estimation, etc. [3,4]. Advances in computational sensing have made NLOS approaches through different methods, and NLOS tracking problems are substantially simpler than reconstructing complete structure information. Meanwhile, compared with active NLOS sensing techniques using streak cameras [5] and single-photon detectors [6,7], the passive NLOS imaging method has the merits of relatively low-cost setups and simple hardware complexity [8–10]. Several passive NLOS sensing methods are proposed for tracking a moving object. They are based on frame cameras and use simulated light transport [11] or speckle imaging [12]. The analysis-by-synthesis approach needs system priors to calibrate the tracking model, and the final results are susceptible to external environmental influences. In addition, it is also required for the speckle imaging method to first calculate the ratio images to extract the primary speckle component. Meanwhile, the existing frame-based methods are easily influenced by environmental parameters, resulting in these prior assumptions often being violated in practical applications.

For a typical passive NLOS tracking method, the camera with an imaging lens is employed to image the relay surface. The captured images by the traditional camera are mixed with the useful speckle grains and background items of the relay surface, which is the major cause of vulnerability to contextual influences. Furthermore, the background items of the relay surface will cause the interference of NLOS object reconstruction, at least two measured images are needed to calculate the energy spectrum, and more images are required to improve it [13]. In practical NLOS scenarios, there are not only different roughness relay surfaces and motion states of the hidden object but also ambient light noise, which will bring more disturbance and unstable elements to traditional frame-based methods. Therefore, alleviating the limitation of background interference is crucial and a challenge for the fast and efficient NLOS tracking task.

In contrast to conventional frame-based cameras, by mimicking how human eyes work, event cameras have the advantages of high temporal resolution, high dynamic range, low redundancy, and low latency, where pixels are triggered asynchronously and independently once the observed luminance changes over a threshold [14–16]. Therefore, computational neuromorphic imaging (CNI) event cameras are suitable for specific optical applications, such as speckle imaging to promote movement detection [17–19]. In particular, they do not react to the static background signal and are highly sensitive to the intensity changes in the speckle field. Hence, there is a significant potential for an event camera to detect moving objects, including the application of NLOS sensing.

In this Letter, an efficient tracking method is proposed for the NLOS moving object with the CNI framework, which is focused on the key element of motion information and is exempt from the disturbance of background items. Leveraging the advanced response characteristics of bio-inspired neuromorphic devices, the CNI-informed NLOS tracking method is efficient via directly using the event stream data and rapidly resolving the motion information. Experimental results demonstrate that the event-based solution is efficient for NLOS motion estimation, which is more applicable for practical continuous tracking.

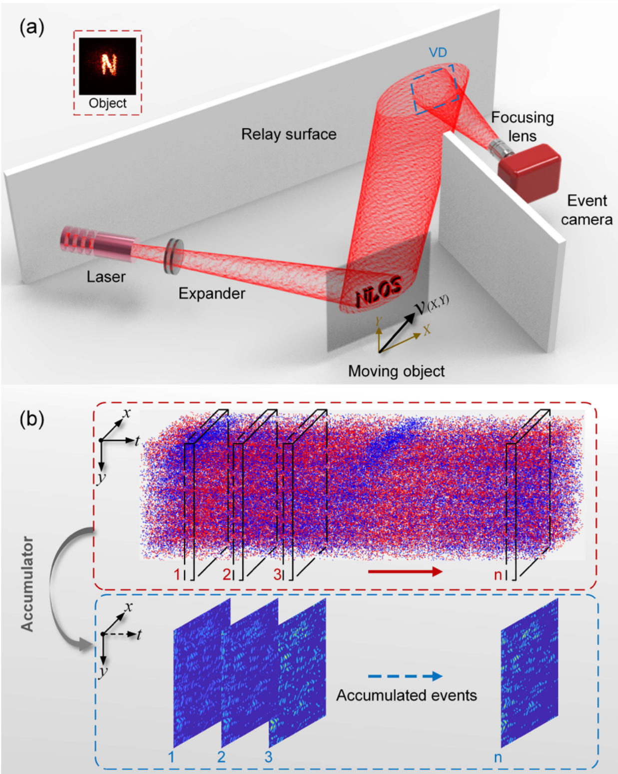

Fig. 1. Hardware implementation and event stream preprocessing. (a) Experimental setup for object moving tracking around the corner. (b) Collected event streams and the 2D integrated speckle patterns through the accumulation step. The transverse direction of the event stream data represents the time changes.

As illustrated in Fig. 1(a), the neuromorphic NLOS tracking model is designed by integrating NLOS inverse correlography with an event generation model. A fraction of the light incident on the object is redirected toward the relay surface, which we call the virtual detector (VD). While a lensless camera is placed on the VD position to directly collect speckle grains, the NLOS inverse process can be simplified as a speckle correlography model, which is an optical technique that allows for the creation of high-resolution images of the diffuse objects [20,21]. Each realization of the generated speckle pattern $I(u)$ in the VD position can be expressed as the squared modulus of the Fourier transform of the complex object field [22]:

$$I(u) = \left|\mathcal{F}\left\{f(x)\right\}\right|^2, \tag{1}$$

where $\mathcal{F}$ denotes a Fourier transform and $f(x)$ is the field reflected by the diffuse object [22]. u denotes a 2D coordinate in the VD plane, and x denotes a 2D spatial coordinate vector in the object space. Coherent light becomes scrambled when encountering a disorder, causing a collimated beam of light transmitted around a rough surface to emerge as a collection of bright and dark spots, commonly referred to as speckles. Although speckle grains may appear random, they actually retain information about the incident object field through correlations. One prominent manifestation of this phenomenon is known as the optical memory effect (OME) [1]. The NLOS tracking task can be described as a rigid body motion of the hidden induced spatial variations in the speckles observed at the VD plane [23]. Within the OME range, the lensless speckle correlography system can be treated as a translational invariance system, allowing for the calculation of object motion through cross-correlation analysis of two speckle patterns (i.e., I_1 and I_2) [18]. The cross-correlation between I_1 and I_2 is equal to that between the object at two different positions. The mathematical expression is as follows: [24]

$$I_1 \star I_2 = (O_1 \star O_2) + C, \tag{2}$$

where the symbol $\star$ denotes the correlation operator; O_1 and O_2 refer to the intensity distribution of the hidden object before and after the movement, respectively; and C is the constant noise term. However, when we collect the frame-based speckles with a focusing lens depicted in Fig. 1(a), it becomes indispensable to consider the background elements present on the relay surface. To measure the fine displacements of objects through cross-correlation, extracting the primary component beforehand is of utmost importance [12].

Therefore, an event camera is employed to mitigate the impact of background elements and directly obtain non-redundant data about the object displacement. Speckle gains will correspondingly shift as the object moves, and events $e_k = (x_k, y_k, t_k, p_k)$ will be generated when the brightness changes of each pixel reach the threshold. As shown in Fig. 1(b), a 2D intensity image can be integrated by accumulating the event streams with a certain time duration Δt, which is expressed as [18]

$$I_{events} = \sum_{t_k \in \Delta t} p_k T \delta(x - x_k, y - y_k), \tag{3}$$

where T denotes the threshold, $p_k \in \{-1, 1\}$ is the event polarity standing for the brightness change, and δ is a Kronecker delta function. In the proposed setup, the event camera focuses on the VD plane, the relay surface is static, and the variable elements are introduced by moving speckles. Consequently, the stationary background items have a minimal impact on the movement information. The collected events and their corresponding accumulated event images can be directly utilized for the cross-correlation operation.

To accurately resolve the degraded movement information of a hidden object, it is essential to exclude the redundant signals (i.e., components of the static relay surface) and extract the primary speckles for motion estimation. As illustrated in Figs. 2(a) and 2(b), a lensless camera system has been incorporated for comparison, which directly captures speckles at the VD position. In other words, a speckle correlography system is utilized to analyze correlative properties. As shown in Figs. 2(c)–2(f), a series of displacement images are practically collected to analyze the influence of the relay surface. For the lensless speckle correlography system, the frame-based speckle patterns can be directly obtained, and the event-based images are calculated by the accumulated step. Then, the correlation coefficients between the initial position and the displacement are correspondingly evaluated, and their comparison results are depicted together in Fig. 2(g). The same as the lensless scattering system, the frame-based spackles and event-based accumulations are collected from the NLOS inverse correlography system. In a scattering system with a steady-state modulation process, the presence of the OME leads to a gradual decline in the correlation coefficient. Typically, the range is defined when the correlation coefficient falls below 0.5 and the values are relatively small in a practical system [25]. For the lensless speckle correlography system, the depicted lines and correlation coefficient have a similar trend. Meanwhile, the same conclusion can be drawn

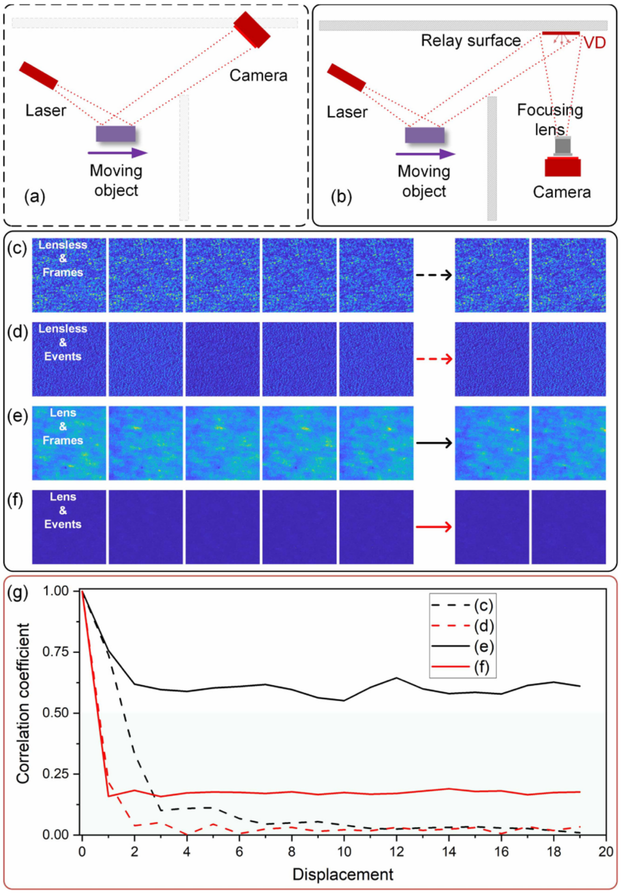

Fig. 2. Analysis of the background items. (a) Lensless speckle correlography system. (b) NLOS inverse correlography system. In order from top to bottom, each line is (c) frame-based lensless speckles, (d) event-based lensless accumulations, (e) frame-based NLOS speckles, and (f) event-based NLOS accumulations. (g) Correlation coefficient in different conditions between the initial position and the displacement. The dash lines represent the patterns from the lensless system and the solid lines represent the patterns from the NLOS system with a focusing lens.

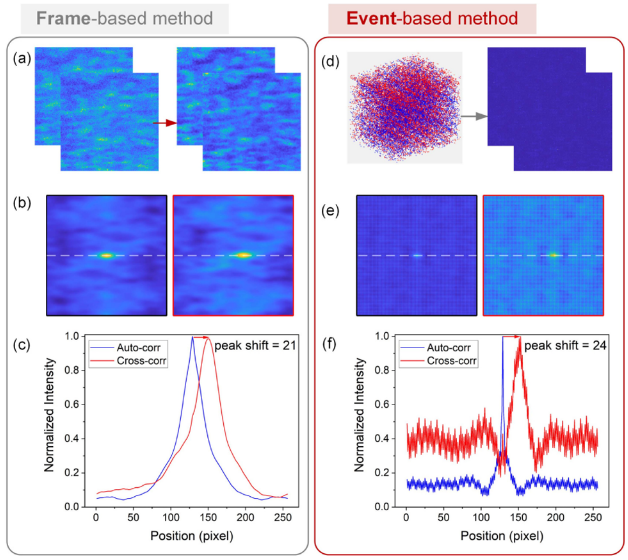

Fig. 3. Comparison results of the frame-based and event-based method. (a) Two adjacent frames and corresponding ratio images. (b) Auto-correlation result of the first ratio image and cross-correlation result of the two ratio images. (c) Intensities of the white dash line in subfigure (b). (d) Event data and corresponding accumulated images. (e) Auto-correlation result of the first accumulated image and cross-correlation result of the two accumulated images. (f) Intensities of the white dash line in subfigure (e).

with the event-based NLOS accumulations, which have a lens focusing on the relay surface. However, the frame-based NLOS speckles have a stronger relevance and present serious hysteresis with the relay surface. Therefore, the influence of the statics relay surface can be ignored by leveraging the specific response characteristics of neuromorphic sensors.

To demonstrate the efficiency of our event-based method, a practical system is developed to collect both frames and event data. As illustrated in Fig. 1(a), the experimental setup of the NLOS tracking includes an illumination light source (Thorlabs, HNL100L) that is a HeNe laser with a wavelength of 632.8 nm and a maximum power of 10 mW. A beam expander spreads the light evenly over the object motion area. A diffuse reflective object is selected as the hidden object and is mounted on the linear translation stage (WN262TA20, Winner Optics). It can move in a 2D plane that is parallel to the relay surface. An event camera (iniVation, DAVIS 346, 346×260 pixels, Events & Frames output) and a focusing lens (Newport, M-20X, 0.4 NA) are employed to collect event stream speckles. In the accumulation process of practical event stream data, the time duration Δt is set as 4×10^5 µs. The frame exposure time is the same as the event accumulation time and the frame interval is set to be zero, for a fair comparison with the event-based method. Images involved in the calculation are selected in a 256×256 pixel size.

The comparison results of the frame-based and event-based approaches are presented in Fig. 3. To compare the displacement more intuitively and calculate the peak shift simply, the intensity in the dash line of auto-correlation and cross-correlation is first normalized. For the NLOS tracking using the frame-based method, we calculate the ratio image and extract the primary speckles for motion estimation [12]. The collected frames are included throughout the object motion, which makes it difficult to calculate the accurate ratio image. Thus, the peak shift of the cross-correlation is hysteretic, and the tracking results are inaccurate. The precise estimation of the primary speckle component and the removal redundancy of the relay surface is crucial for the frame-based method, which is also a limitation for the practical application of the frame-based approach. Leveraging the advanced response characteristics of neuromorphic sensors, the event camera only reacts to the brightness changes of moving speckle grains and has little response to the static relay surface. The collected spatiotemporal event streams have no redundant information about the static relay surface and can thus be directly employed in motion estimation. As shown in Fig. 3(f), the correlation results have a sharp curve, which is more suitable for quantifying the object displacement. Therefore, by using non-redundant events, more accurate cross-correlation results can be obtained. More results of 1D continuous motion with different materials, speeds, illumination intensities, and ambient light are shown in Supplement 1. The event-based method can also promote the capability of further subdividing displacements with high temporal resolution properties (see Supplement 1).

To further verify the effectiveness of our method, a comparative study for measuring continuous movement is conducted.

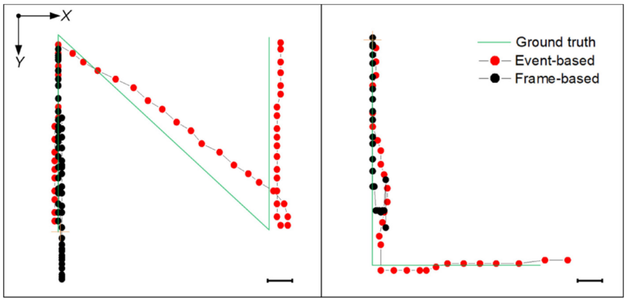

Fig. 4. Experimental results showcase continuous motion estimation, with trajectory reconstructions resembling the letters "N" and "L", respectively. Scale bars: 0.05 mm.

In the experiments, both speckle events and frames throughout the motion process of the concealed object are simultaneously collected. To analyze the difference between the two methods, full frames with specific trajectories are utilized for ratio image calculation. The motion trajectories of the object are configured as the letters "N" and "L". As shown in Fig. 4, two different trajectories are designed for NLOS movement sensing. The conclusive results of trajectory reconstruction reveal that the event-based method yields reliable NLOS tracking results, whereas the frame-based method fails to estimate the motion accurately. Meanwhile, the CNI-informed NLOS tracking method is also robust to the sensing scenes, such as the light condition and the characteristics of the hidden object (see Supplement 1).

It should be noted that the experimental system is subject to non-idealities, such as the event camera's sensitivity to environmental interference, particularly vibrations and instability of the translation stage. Consequently, the practical tracking results may exhibit deviations from the original trajectory settings. Due to the hysteresis effect with background interference, the tracking results have more delay via the frame-based approach. The vertical component is larger than the horizontal component with our designed trajectory. As well as the larger motion components along the vertical direction (Y-direction) than the horizontal direction (X-direction), the estimated results along the horizontal direction are further degraded when using an uncalibrated frame-based method. The tracking accuracy of the NLOS tracking via the event-based method is also influenced by several factors, e.g., the quality of collected speckle events, an appropriate time-duration section, and the stability of system implementation. Meanwhile, it is worth noting that existing commercial event cameras have a relatively lower spatial resolution, making it challenging to reconstruct the complete structural information. For future studies, the incorporation of additional optical techniques and computational methods can be explored to further improve the signal-to-noise ratio in the inverse correlography model, e.g., event warping [26] and compressive coding [27].

In conclusion, we propose a neuromorphic NLOS tracking method that enables direct and precise estimation of motion information and circumvents the relay surface disturbance. By leveraging non-redundant events, the accuracy and efficiency of NLOS tracking can be further improved than traditional frames. The neuromorphic NLOS tracking technique paves the way for future research that could go beyond hidden shape reconstruction to object detection, target recognition, or other sensing tasks, providing valuable insights for sensing applications ranging from low-level to high-level complex scenarios.

Funding. Research Grants Council of Hong Kong (GRF 17201620); ACCESS — AI Chip Center for Emerging Smart Systems, sponsored by InnoHK funding, Hong Kong SAR; National Natural Science Foundation of China (61971227, 62031018).

Acknowledgment. We thank Jianqing Huang, Kaiqiang Wang, Pei Zhang, and Wenjun Zhang for their suggestions and technical support.

Disclosures. The authors declare no conflicts of interest.

Data availability. Data underlying the results presented in this Letter are not publicly available at this time but may be obtained from the authors upon reasonable request.

Supplemental document. See Supplement 1 for supporting content.

REFERENCES

1. J. Bertolotti, E. G. Van Putten, C. Blum, *et al.*, Nature **491**, 232 (2012).
2. T. Maeda, G. Satat, T. Swedish, *et al.*, "Recent advances in imaging around corners," arXiv, arXiv:1910.05613 (2019).
3. D. Faccio, A. Velten, and G. Wetzstein, Nat. Rev. Phys. **2**, 318 (2020).
4. K. L. Bouman, V. Ye, A. B. Yedidia, *et al.*, in *Proceedings of the IEEE International Conference on Computer Vision* (2017), pp. 2270–2278.
5. A. Velten, T. Willwacher, O. Gupta, *et al.*, Nat. Commun. **3**, 745 (2012).
6. C. A. Metzler, D. B. Lindell, and G. Wetzstein, IEEE Trans. Comput. Imaging **7**, 1 (2021).
7. X. Liu, J. Wang, L. Xiao, *et al.*, Nat. Commun. **14**, 3230 (2023).
8. C. Saunders, J. Murray-Bruce, and V. K. Goyal, Nature **565**, 472 (2019).
9. F. Willomitzer, P. V. Rangarajan, F. Li, *et al.*, Nat. Commun. **12**, 6647 (2021).
10. Y. Shi, W. Sheng, Y. Fu, *et al.*, Nat. Commun. **14**, 7742 (2023).
11. J. Klein, C. Peters, J. Martín, *et al.*, Sci. Rep. **6**, 32491 (2016).
12. B. M. Smith, M. O'Toole, and M. Gupta, in *in Proceedings of the IEEE Conference on Computer Vision and Pattern Recognition* (2018), pp. 6258–6266.
13. C. A. Metzler, F. Heide, P. Rangarajan, *et al.*, Optica **7**, 63 (2020).
14. G. Gallego, T. Delbrück, G. Orchard, *et al.*, IEEE Trans. Pattern Anal. Mach. Intell. **44**, 154 (2022).
15. Z. Ge, H. Wei, F. Xu, *et al.*, Opt. Lasers Eng. **160**, 107247 (2023).
16. P. Zhang, Z. Ge, L. Song, *et al.*, IEEE Trans. Comput. Imaging **9**, 530 (2023).
17. S. Zhu, C. Wang, H. Liu, *et al.*, *Computational Optical Imaging and Artificial Intelligence in Biomedical Sciences*, Vol. 12857 (SPIE, 2024), pp. 4–10.
18. Z. Ge, Y. Gao, H. K.-H. So, *et al.*, Opt. Lett. **46**, 3885 (2021).
19. C. Wang, Y. He, X. Wang, *et al.*, Chin. Opt. Lett. **21**, 061103 (2023).
20. A. Viswanath, P. Rangarajan, D. MacFarlane, *et al.*, in *Computational Optical Sensing and Imaging* (2018), pp. CM2E–3.
21. M. M. Balaji, J. Liu, D. Ahsanullah, *et al.*, Opt. Express **31**, 21689 (2023).
22. J. R. Fienup and P. S. Idell, Opt. Eng. **27**, 778 (1988).
23. P. Jacquot and P. K. Rastogi, Appl. Opt. **18**, 2022 (1979).
24. C. Guo, J. Liu, T. Wu, *et al.*, Appl. Opt. **57**, 905 (2018).
25. S. Zhu, E. Guo, J. Gu, *et al.*, Photonics Res. **9**, B210 (2021).
26. G. Gallego, H. Rebecq, and D. Scaramuzza, in *in Proceedings of the IEEE Conference on Computer Vision and Pattern Recognition* (2018), pp. 3867–3876.
27. J. Ke, L. Zhang, Q. Zhou, *et al.*, Opt. Express **29**, 5710 (2021).